Catalysis Today 164 (2011) 62–67

Contents lists available at ScienceDirect

Catalysis Today

journal homepage: www.elsevier.com/locate/cattod

Identification of the active species in the working alumina-supported cobalt catalyst under various conditions of Fischer–Tropsch synthesis

M. Sadeqzadeh[a], H. Karaca[a], O.V. Safonova[b,*], P. Fongarland[a], S. Chambrey[a], P. Roussel[a], A. Griboval-Constant[a], M. Lacroix[c], D. Curulla-Ferré[d], F. Luck[d], A.Y. Khodakov[a,**]

[a] Unité de Catalyse et de Chimie du Solide (UCCS), UMR 8181 CNRS, Université Lille 1-ENSCL-EC-Lille, Cité scientifique, Bât C3, 59655 Villeneuve d'Ascq, France
[b] Swiss-Norwegian Beamlines, ESRF, BP 220, 38043 Grenoble Cedex, France
[c] Total Petrochemicals Research Feluy, 7181 Seneffe, Belgium
[d] Total S.A., 2 Place Jean Millier, 92078 Paris la Défense Cedex, France

ARTICLE INFO

Article history:
Received 1 July 2010
Received in revised form
14 December 2010
Accepted 15 December 2010
Available online 15 January 2011

Keywords:
Clean fuels
Catalyst restructuring
Fischer–Tropsch synthesis
Cobalt
In situ

ABSTRACT

An *in situ* time-resolved XRD/XANES/EXAFS investigation combined with on-line evaluation of catalytic performance indicates considerable structural transformations of the conventional Pt-promoted alumina supported cobalt catalyst under the realistic conditions of Fischer–Tropsch synthesis. Cobalt and platinum are reduced into metallic states after pre-treatment in hydrogen at 623 K and form Co–Pt bimetallic nanoparticles. Depending on catalyst and reaction conditions, the metallic nanoparticles can undergo sintering, carbidisation, and *fcc–hcp* phase transformations. The observed changes in the catalyst structure significantly affect the performance in the Fischer–Tropsch reaction. Cobalt *hcp* phase seems more active in Fischer–Tropsch synthesis than cobalt *fcc* metal phase.

1. Introduction

The recent resurgence of interest in alternative fuels is primarily due to the growing global demand for clean energy. The alternative ultra-clean fuels can be manufactured from biomass (BTL), coal (CTL), and natural gas (GTL) using Fischer–Tropsch technology (FT) [1]. FT reaction occurs on supported cobalt catalysts. Alumina supported cobalt catalysts are currently used commercially in several industrial FT projects. For cobalt particles larger than 6–8 nm FT reaction rate is considered to be structure independent and normally is proportional to the density of surface cobalt atoms in the catalyst. The reaction rate typically decreases with time-on-stream due to catalyst deactivation [2]. The deactivation rate depends on catalyst, catalytic reactor and operating conditions. The efficient control of FT deactivation under industrially relevant conditions is crucial to attain high and enduring hydrocarbon productivity.

The literature exhibits a large divergence concerning the mechanisms of deactivation of cobalt FT catalysts. The discrepancies are principally related to the lack of direct catalyst characterization techniques [3]. Indeed, the structure of cobalt catalysts evolves during the reaction and is very sensitive to the reaction conditions [4]. In addition, cobalt species could be readily oxidized in air after catalyst withdrawal from the reactor. Hence, reliable information about the mechanism of catalysts deactivation could be only obtained by using *in situ* direct characterization techniques conducted under the representative conditions of FT synthesis. Direct *in situ* characterization of catalyst structure under realistic FT reaction conditions represents a significant experimental challenge [5,6] because of high temperature, high pressure, presence of a large number of reaction products, multiphase reacting medium, etc. Most of the previous studies on deactivation of cobalt catalysts have been conducted either *ex situ* or *in situ* under conditions far from those typically used during FT industrial process. The *in situ* studies under conditions relevant to FT industrial process have become possible only very recently [5,6].

The structural studies utilizing synchrotron radiation are well suited for *in situ* time-resolved measurements of catalysts, as the high brilliance of modern synchrotron sources allows fast acquisition of X-ray scattering and X-ray absorption spectra even for diluted systems inside catalytic reactor cells. The present paper focuses on the *in situ* time-resolved XRD/XAS investigation of the cobalt active sites in a conventional alumina supported catalyst at a wide range of the experimental conditions relevant to FT synthe-

* Corresponding author. Present address: Paul Scherrer Institut, CH 5232 Villigen PSI, Switzerland. Tel.: +41 56 310 5805.
** Corresponding author. Tel.: +33 320335439; fax: +33 320436561.
E-mail addresses: olga.safonova@psi.ch (O.V. Safonova), andrei.khodakov@univ-lille1.fr (A.Y. Khodakov).

0920-5861/$ – see front matter © 2010 Elsevier B.V. All rights reserved.
doi:10.1016/j.cattod.2010.12.035

sis. The characterization was combined with on-line evaluation of the catalytic performance using gas-chromatography. The *in situ* experiments were conducted using syngas with H_2/CO ratios from 0.5 to 4 and at temperatures 493–523 K.

2. Experimental

A cobalt $CoPt/Al_2O_3$ catalyst was synthesized via co-impregnation of Puralox SCCA-5/170 alumina (Sasol, S_{BET} = 165 m^2/g, pore diameter 8.3 nm and total pore volume 0.477 cm^3/g) using aqueous solutions of cobalt nitrate and tetrammine platinum nitrate. The cobalt and platinum contents in the catalyst were respectively 25 wt.% and 0.1 wt.%. The impregnated solid was calcined in air flow at 573 K and reduced in hydrogen at 623 K. The catalyst has been characterized *ex situ* by a wide range of techniques: BET, XRD, TPR, TEM–EDX, and STEM–EELS.

The *in situ* time-resolved XRD and XAS data were measured simultaneously at the BM01B beamline (ESRF, France). 5–10 mg of catalyst was loaded in the quartz capillary reactor (OD = 1 mm, wall thickness = 0.020 mm) and pressed from both sides with quartz wool. A Cyberstar gas blower was used to control the reactor temperature. A gas manifold system and a capillary reactor are described elsewhere [5,6]. Before FT reaction all the catalyst samples were reduced *in situ* under flow of pure H_2 (P = 1 bar) during the temperature ramping (3 K/min) up to 623 K and then cooled down to 333 K in H_2 flow. Then the syngas was introduced, the reactor was pressurized up to 20 bar and the catalyst was heated in the gas flow up to the desired temperature. XRD patterns were acquired using a monochromatic X-ray beam (Si 1 1 1 channel-cut monochromator, λ = 0.05 nm) and a high-resolution diffractometer. Each XRD pattern (2θ range: 2–22°) was measured for 10 min. *In situ* XAS spectra at Co K-edge and Pt L_3-edge were acquired using Si 1 1 1 double crystal monochromator (detuned to 50%) in fluorescence mode (Vortex Silicon drift detector). The data analysis was performed applying the IFFEFIT software [7]. Each XANES spectrum at Co K-edge (from 7600 to 8000 eV) was collected for 5 min. Since the concentration of cobalt in the catalyst was rather high (25 wt%), XAS data were corrected for the self-absorption using the atoms algorithm as implemented in the ATHENA program [8]. Due to low concentration of Pt in the catalyst (0.1 wt%) XAS data at Pt L_3-edge (from 11,500 eV to 12,500 eV) were measured for 4 h under under hydrogen flow (after reduction at 623 K). The EXAFS data were normalized to the edge jump of 1 over the range of 150–930 eV above the edge position. The data in R-space are obtained via Fourier transformation (k = 2–10 $Å^{-1}$, dk = 1, Hanning window, k weight = 3). The fit of the first coordination shell is performed in the R space at k weight = 3 for k range = 2–10 $Å^{-1}$ and R = 1–3 Å.

Simultaneous analysis of the FT reaction products was conducted using an Agilent micro gas-chromatograph. The gas lines were heated up to 473 K to preheat the reacting gases and to prevent condensation of liquid products. The liquid and solid products were collected downstream of the reactor. The performance of the alumina supported cobalt catalyst was also studied under steady-state conditions in a conventional laboratory-scale fixed bed reactor (d_{int} = 13, m_{cat} = 1 g diluted in carborundum). Before the FT tests in both capillary and conventional fixed bed reactors, the catalyst was reduced in hydrogen flow at 623 K at atmospheric pressure (temperature ramp of 3 K/min). In laboratory scale fixed bed reactor at 493 K, H_2/CO = 2 and P = 20 bar, cobalt catalyst exhibited cobalt time yield of $\sim 5 \times 10^{-3}$ s^{-1} with 8% methane selectivity at 40% carbon monoxide conversion. The observed catalytic performance is consistent with previous data [9–11].

3. Results and discussion

3.1. Cobalt and platinum reduction, formation of Co–Pt mixed particles

The *in situ* XRD patterns of calcined and reduced catalyst are shown in Fig. 1. The XRD patterns of the calcined catalyst are indicative of the presence of Co_3O_4 crystallites and γ-alumina phase. The size of Co_3O_4 crystallites calculated using the Scherrer equation was about 10 nm. The TEM and STEM–EELS images (not shown) show the presence of cobalt oxide particles with diameter between 5 and 15 nm. The *in situ* XRD suggests that cobalt reduction is nearly complete at 623 K. According to Rietveld analysis, cobalt was mainly present in the form of *fcc* metallic phase (80% cobalt *fcc* and 20% *hcp* phases).

The Co K-edge XANES spectra of the catalyst after reduction in H_2 at 623 K together with CoO and Co foil reference compounds are shown in Fig. 2. Co K-edge in the reduced catalyst exhibits very low intensity of the white line that is typical for the metallic state. The evolution of cobalt oxidation state measured on-line during catalyst reduction is given in Fig. 3. These data are obtained from decomposition of the catalyst XANES spectra using linear combination of XANES spectra of Co, CoO and Co_3O_4 reference compounds. As shown previously [12,13], cobalt reduction proceeds via intermediate formation of CoO which was observed as the major phase between 473 K and 543 K. In agreement with XRD data, XANES at

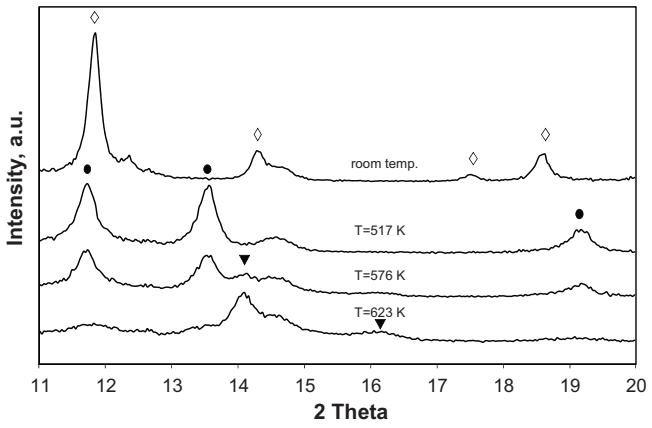

Fig. 1. *In situ* XRD patterns (λ = 0.05 nm) of $CoPt/Al_2O_3$ measured at different temperatures during the reduction in hydrogen (λ = 0.05 nm; ◊, Co_3O_4; ●, CoO; ▼, metal Co *fcc*).

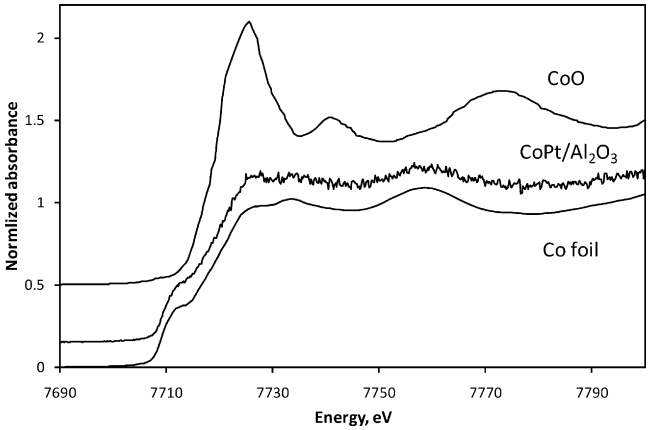

Fig. 2. *In situ* XANES spectra of $CoPt/Al_2O_3$ after reduction with hydrogen at 623 K, CoO and Co foil reference compounds.

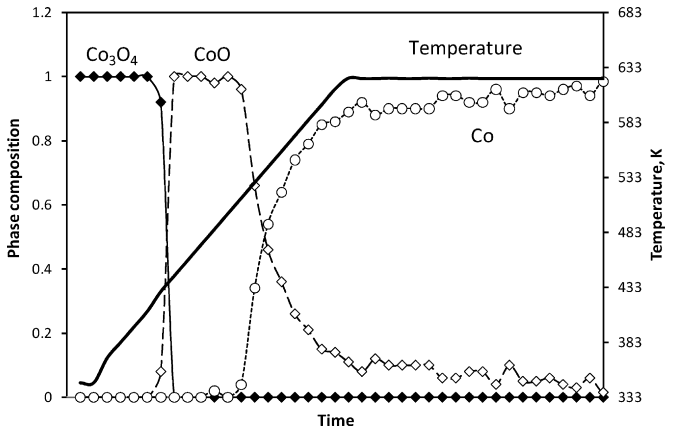

Fig. 3. Cobalt phase composition of $CoPt/Al_2O_3$ catalyst during the reduction in hydrogen calculated from XANES data.

Co K-edge shows nearly complete cobalt reduction after catalyst treatment with hydrogen at 623 K.

Fig. 4a shows the *in situ* XANES spectra measured at Pt L_3-edge after reduction of the catalyst in hydrogen at 623 K. Low intensity of Pt L_3 white line in reduced state indicates the presence of Pt metallic species. The shape of Pt L_3 edge in the reduced catalyst is different from that of Pt foil. The EXAFS Fourier transform modulus (Fig. 4b) exhibits a peak at shorter distances than in Pt–Pt coordination sphere. These experimental observations are consistent with

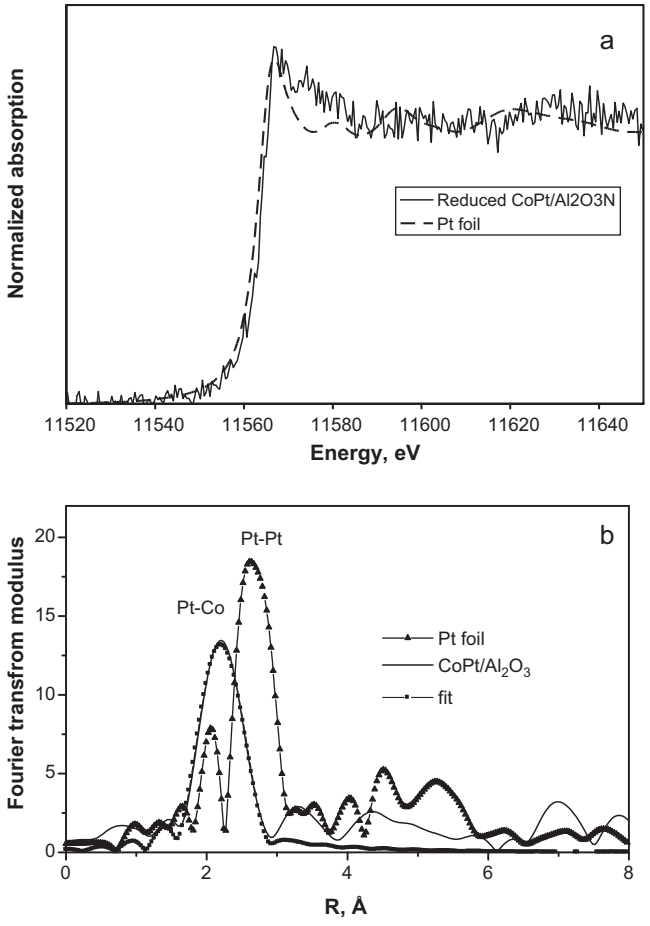

Fig. 4. *In situ* XANES spectra (a) and k^3 EXAFS Fourier transform moduli (b) of $CoPt/Al_2O_3$ reduced at 623 K and Pt foil at Pt L_3 absorption edge. The displayed fit assumes Pt coordination with Co atoms.

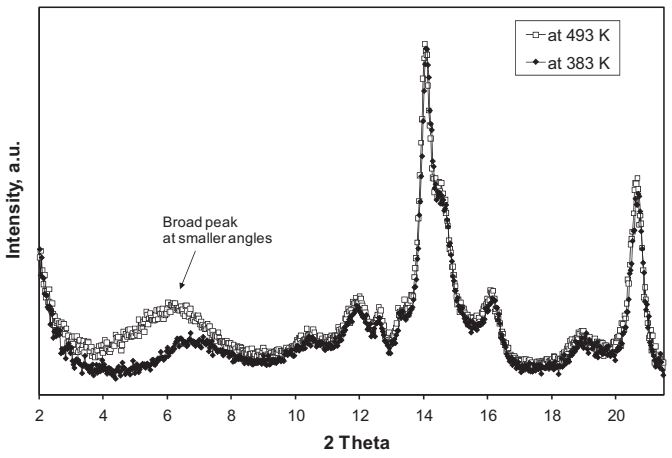

Fig. 5. *In situ* XRD patterns ($\lambda = 0.05$ nm) of $CoPt/Al_2O_3$ catalyst in syngas at 383 K (no FT reaction) and at 493 K at $H_2/CO = 0.5$ ($P = 20$ bar).

previous report by Davis and co-workers [14]. The EXAFS spectrum of platinum in reduced catalyst cannot be fitted successfully having Pt atoms in the first coordination shell. The fit improves when cobalt is present in the first coordination shell of platinum. The results of the fit shown in Fig. 4b are the following: $R_{Pt-Co} = 2.56(\pm 0.01)$ Å, $N_{Pt-Co} = 11.7(\pm 1.5)$, $E_o = 8.29(\pm 1.5)$ eV, $\sigma^2 = 0.011(\pm 0.001)$ Å^2, number of independent points = 10, number of variables = 4. The Pt–Co coordination distance obtained in our experiment corresponds well to the crystallographic data of Pt–Co bimetallic compounds [15]. It indicates that after reduction of the catalyst in hydrogen Pt dissolves in the structure of cobalt nanoparticles forming bimetallic structure.

3.2. Evolution of cobalt catalysts under syngas with different H_2/CO ratios

The *in situ* XRD patterns of the reduced $CoPt/Al_2O_3$ catalysts measured under different conditions relevant to FT synthesis are shown in Figs. 5 and 6. Exposure of the catalyst to syngas results in appearance of a broad peak at low angles (around 6°), which is typical of amorphous phases and liquids (Fig. 5). The intensity of this peak changes as a function of CO/H_2 ratio in the syngas used for FT synthesis: it increases when syngas has low $H_2/CO = 0.5$ ratio and drops to zero under the conditions favoring methanation ($H_2/CO = 4$). Since the concentration of liquid hydrocarbons is usually more significant when the feed has a H_2/CO ratio ≤ 2, the origin peak is probably relevant to the accumulation of the liquid phase in the catalyst bed. The decrease in the total pressure in the *in situ* reaction cell results in the disappearance of this broad peak, which can be explained by evaporation of hydrocarbons.

Fig. 6 shows evolution of the *in situ* cobalt XRD patterns during FT reaction using syngas with different H_2/CO ratios. The XRD peaks attributed to cobalt *fcc* phase are getting narrower with increasing reaction time. Analysis of the evolution of XRD patterns using full profile matching suggests an increase in the sizes of cobalt metal crystallites, i.e. cobalt sintering during the reaction. Cobalt sintering occurs during the initial period of the reaction and is more significant when syngas had higher H_2/CO ratio (Fig. 6b and c, $H_2/CO = 2$–4). Note the upper size of cobalt crystallites after sintering is limited by the support pore diameter in alumina (~8 nm). Integration of XRD patterns (Fig. 6) did not show any decrease in the intensity of XRD peaks attributed to cobalt metal phase or any increase in the intensity of cobalt oxide XRD patterns during FT reaction. This suggests that no cobalt oxidation is observed at moderate carbon monoxide conversions (<20%) in the catalysts with cobalt *fcc* crystallites of 6–10 nm. Simultaneously conducted

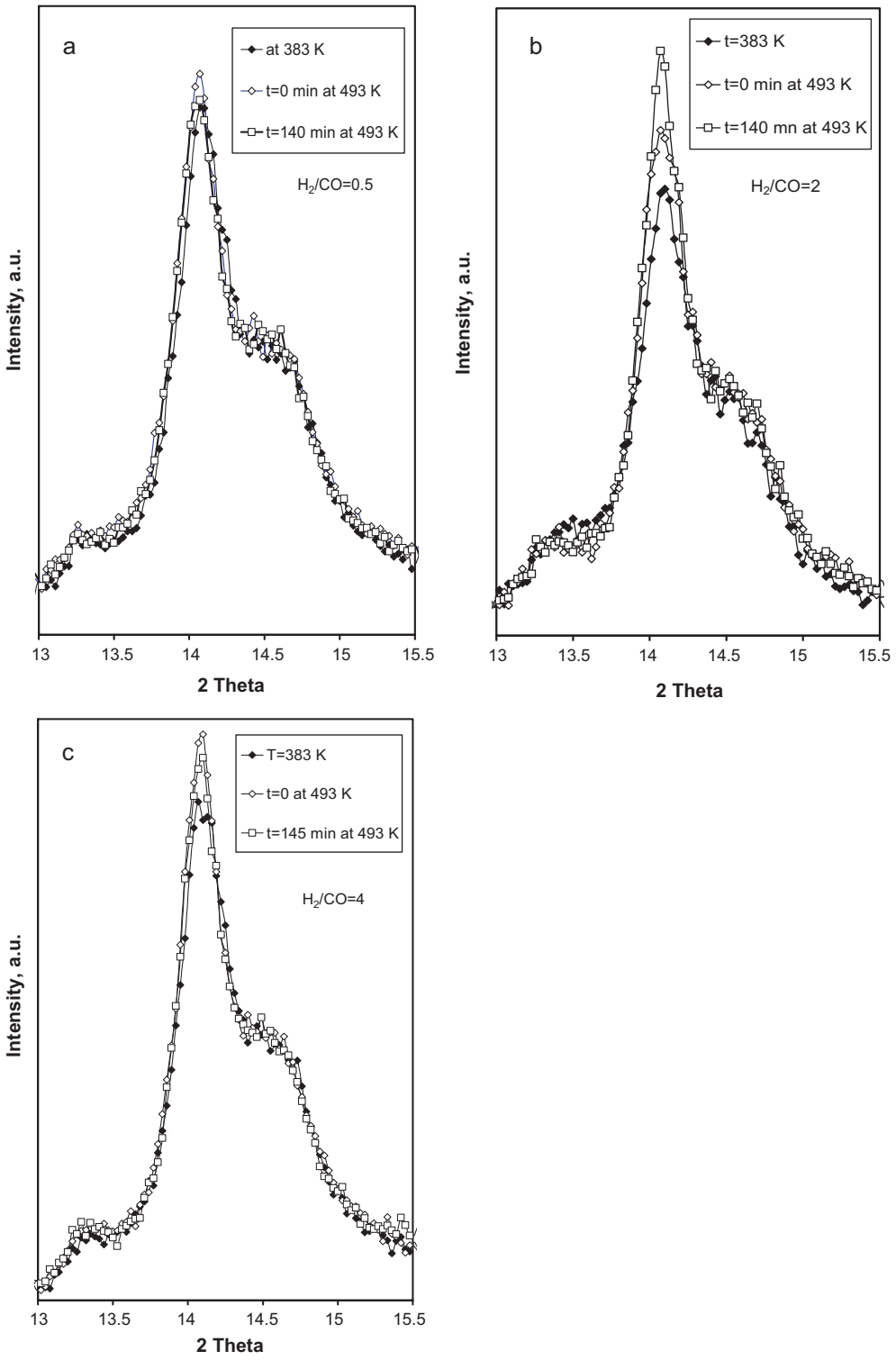

Fig. 6. Evolution of the cobalt *fcc* peaks in the *in situ* XRD patterns ($\lambda = 0.05$ nm) of $CoPt/Al_2O_3$ catalyst during FT reaction using syngas with $H_2/CO = 0.5$ (a), $H_2/CO = 2$ (b) and $H_2/CO = 4$ (c) ratios ($P = 20$ bar, $T = 493$ K).

analysis of reaction products uncovered a decrease in carbon monoxide conversion from 60% to 20% at GHSV = 25 000 ml g^{-1} h^{-1} and $H_2/CO = 2$.

The stability of cobalt metal particles was studied in wet argon, wet hydrogen and during FT reaction. In wet argon ($P_{H_2O}/P_{Ar} = 5$, $T = 493$ K, $P = 1$ bar) the *in situ* XAS data were indicative of rapid oxidation of cobalt metal particles, while no bulk cobalt oxidation was observed in hydrogen with higher amounts of water ($P_{H_2O}/P_{H_2} = 3.34$, $P = 1$ bar). The *in situ* XRD experiments conducted during FT synthesis ($H_2/CO = 2$, $P = 20$ bar, $T = 493$ K) with addition of water (up to 50 mol%, $H_2O/H_2 = 1.3$) did not show any noticeable bulk cobalt oxidation for the conventional $CoPt/Al_2O_3$ catalyst containing relatively larger Co crystallites (>6–7 nm). Further details on the influence of effect of water on catalyst structure and catalytic per-

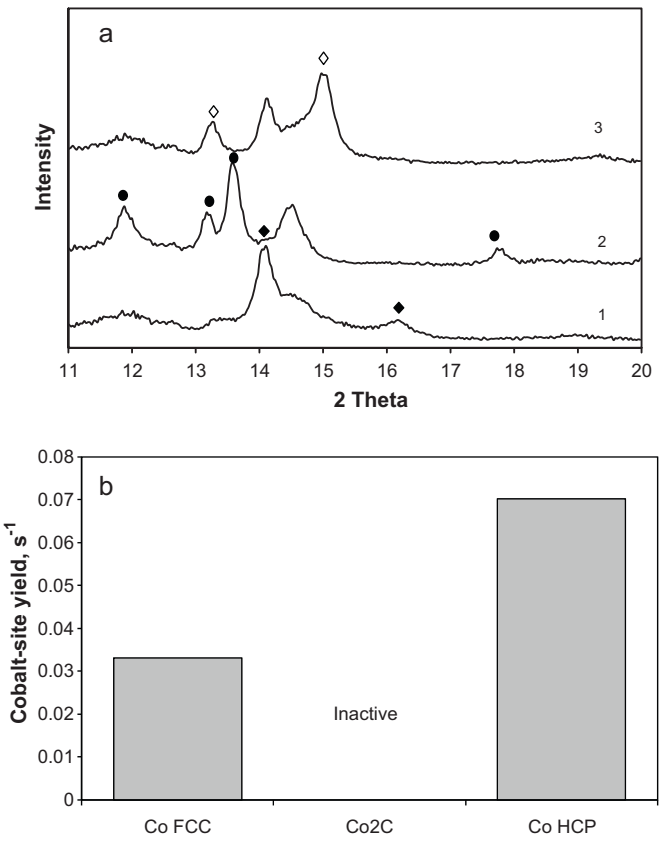

Fig. 7. *In situ* XRD patterns (λ = 0.05 nm) (a) and cobalt-site yields in FT synthesis (b) obtained with $CoPt/Al_2O_3$: (1) after reduction in H_2 resulting in cobalt *fcc* phase, (2) after catalyst exposure to pure CO leading to cobalt carbide (3) after hydrogenation of cobalt carbide to cobalt *hcp* phase (♦, Co *fcc*; ●, Co_2C; ◊, Co *hcp*).

formance are available in our recent publication [16]. The obtained *in situ* data are consistent with the results of thermodynamic calculations by van Steen et al. [17] and previous report by van de Loosdrecht et al. [3] who did not observe any cobalt oxidation during FT synthesis with a commercial catalyst in an industrial slurry bubble column reactor (SBCR).

3.3. Catalyst carbidisation, cobalt fcc and hcp phases

Fig. 7a shows *in situ* XRD patterns obtained during catalysts exposure to pure CO. Catalyst exposure to pure CO rapidly results in formation of Co_2C cobalt carbide, which was clearly identified using *in situ* XRD patterns. The simultaneously conducted catalytic tests showed zero activity of Co_2C phase in FT reaction. Cobalt carbide can however be hydrogenated in hydrogen. Carbide hydrogenation results in selective formation of cobalt hexagonal *hcp* phase (Fig. 7a). Full profile matching analysis uncovered cobalt *fcc* crystallite size of about 7 nm in the conventionally reduced catalysts after several hours of reaction, while the size of cobalt *hcp* crystallites was about 9 nm in the catalysts which were subjected to consecutive carbidisation and hydrogenation. Cobalt-site yields (s^{-1}) were calculated from carbon monoxide conversions, gas flow velocities and normalized by the number of cobalt surface atoms. Cobalt dispersion was estimated assuming spherical uniform cobalt particles with site density of 14.6 atoms/nm^2 and using the formula: $D = 96/d$ [18], where D (%) is cobalt dispersion and d (nm) is cobalt particle size. The catalytic measurements (Fig. 7b) showed higher FT catalytic activity of $CoPt/Al_2O_3$ catalyst, which contained cobalt *hcp* phase, obtained via consecutive carbidisation and hydrogenation. These results were also confirmed by using catalytic tests in conventional laboratory scale fixed bed reactor. The hydrocarbon selectivity was similar with the catalysts containing cobalt *fcc* and cobalt *hcp* phases. Cobalt *hcp* phase exhibited higher cobalt-site yield in FT synthesis than cobalt *fcc* phase. The higher catalytic activity of the catalysts containing cobalt *hcp* phase was observed for several hours in capillary fixed bed reactor with simultaneous measurements of XRD patterns and XAS and for several hundred hours in the conventional laboratory-scale fixed bed reactor. No transformation of cobalt *hcp* into cobalt *fcc* phase was observed under the reaction conditions.

These results are in agreement with previous data by Ducreux et al. [19] who observed higher activity of cobalt *hcp* phase at low pressure and under methanation conditions ($H_2/CO = 9$). Note that the conclusion about higher turnover frequency of cobalt *hcp* phase is based on the spherical morphology. Another possible explanation of higher activity of cobalt *hcp* phase could be related to the porous structure of cobalt *hcp* particles.

4. Conclusion

The *in situ* synchrotron based experiments showed significant evolution of the structure and catalytic performance of cobalt supported catalysts under the realistic conditions of FT synthesis. In the reduced Pt promoted alumina supported cobalt catalysts *in situ* X-ray absorption was indicative of the presence of bimetallic Co–Pt particles. Cobalt sintering which seems to be one of the major mechanisms of catalyst deactivation, depends on the operating conditions. Cobalt sintering seems to be more significant under syngas having higher H_2/CO ratio. In the conventional cobalt catalysts with relatively large cobalt particles (>6–7 nm), cobalt oxidation was not detected at moderate carbon monoxide conversions even in the presence of additional water ($P_{H_2O}/P_{H_2} = 1.3$). Cobalt *fcc* phase was the dominant cobalt phase in the cobalt catalysts reduced in hydrogen. Cobalt *hcp* phase, which can be generated in the catalysts by consecutive CO and H_2 treatments, was found to be more active than the cobalt *fcc* phase.

Acknowledgements

M.S. and H. K. are grateful to TOTAL S.A. for providing PhD fellowships. The authors thank SNBL-ESRF and TOTAL S.A. for technical assistance and financial support. The ESRF is acknowledged for the use of synchrotron radiation.

References

[1] A.Y. Khodakov, W. Chu, P. Fongarland, Chem. Rev. 107 (2007) 1692–1744.
[2] N.E. Tsakoumis, M. Rønning, Ø. Borg, E. Rytter, A. Holmen, Catal. Today 154 (2010) 162–182.
[3] J. van de Loosdrecht, B. Balzhinimaev, J.-A. Dalmon, J.-W. Niemantsverdriet, S.V. Tsybulya, A.M. Saib, P.J. van Berge, J.L. Visagie, Catal. Today 123 (2007) 293–302.
[4] J. Wilson, C. de Groot, J. Phys. Chem. 99 (1995) 7860–7866.
[5] M. Rønning, N.E. Tsakoumis, A. Voronov, R.E. Johnsen, P. Norby, W. van Beek, Ø. Borg, E. Rytter, A. Holmen, Catal. Today 155 (2010) 289–295.
[6] H. Karaca, J. Hong, P. Fongarland, P. Roussel, A. Griboval-Constant, M. Lacroix, K. Hortmann, O.V. Safonova, A.Y. Khodakov, Chem. Commun. 46 (2010) 788–790.
[7] M. Newville, J. Synchrotron Radiat. 8 (2001) 322–324.
[8] B. Ravel, J. Synchrotron Radiat. 8 (2001) 314–316.
[9] P.J. van Berge, J. van de Loosdrecht, J.L. Visagie, International Patent WO 01/39882 A1, assigned to Sasol (7 June 2001).
[10] R. Oukaci, A.H. Singleton, J.G. Goodwin, Appl. Catal. 186 (1999) 129–144.
[11] O. Borg, S. Erib, E.A. Blekkan, S. Storsaeter, H. Wigum, E. Rytter, A. Holmen, J. Catal. 248 (2007) 89–100.
[12] D.G. Castner, P.R. Watson, I.Y. Chan, J. Phys. Chem. 94 (1990) 819–828.
[13] A.Y. Khodakov, J. Lynch, D. Bazin, B. Rebours, N. Zanier, B. Moisson, P. Chaumette, J. Catal. 168 (1997) 16–25.
[14] G. Jacobs, J.A. Chaney, P.M. Patterson, T.K. Das, J.C. Maillot, B.H. Davis, J. Synchrotron Radiat. 11 (2004) 414–422.
[15] K.H.J. Buschow, P.G. van Engen, R. Jongebreur, J. Magn. Magn. Mater. 38 (1983) 1–22.

[16] H. Karaca, O.V. Safonova, S. Chambrey, P. Fongarland, P. Roussel, A. Griboval-Constant, M. Lacroix, A.Y. Khodakov, J. Catal. 277 (2011) 14–26.
[17] E. van Steen, M. Clayes, M.E. Dry, J. van de Loosdrecht, E.L. Vilkoen, J.L. Visagie, J. Phys. Chem. B 109 (2005) 3575–3577.
[18] D. Schanke, S. Vada, E.A. Blekkan, A.M. Hilmen, A. Hoff, A. Holmen, J. Catal. 156 (1995) 85–95.
[19] O. Ducreux, J. Lynch, B. Rebours, M. Roy, P. Chaumette, Stud. Surf. Sci. Catal. 119 (1998) 125–130.